IEEE Access
Multidisciplinary | Rapid Review | Open Access Journal

Received 10 June 2022, accepted 19 July 2022, date of publication 29 July 2022, date of current version 3 August 2022.

Digital Object Identifier 10.1109/ACCESS.2022.3194850

APPLIED RESEARCH

Self-Sustained Rigid Fully Metallic Metasurfaces to Enhance Gain of Shortened Horn Antennas

FOEZ AHMED[1], (Graduate Student Member, IEEE), MUHAMMAD U. AFZAL[1], (Senior Member, IEEE), TOUSEEF HAYAT[2], (Graduate Student Member, IEEE), KARU P. ESSELLE[1], (Fellow, IEEE), AND DUSHMANTHA N. THALAKOTUNA[1], (Senior Member, IEEE)

[1]School of Electrical and Data Engineering, University of Technology Sydney (UTS), Sydney, NSW 2007, Australia
[2]School of Engineering, Macquarie University, Sydney, NSW 2109, Australia

Corresponding author: Foez Ahmed (foez.ahmed@student.uts.edu.au)

This work was supported in part by the Australian Research Council (ARC) Discovery Grant, in part by the University of Technology Sydney Seed Grant, in part by the International Research Scholarship (IRS), and in part by the Faculty of Engineering and Information Technology (FEIT) Scholarship.

ABSTRACT This article presents mechanically robust, low-cost, lightweight, and polarization-independent metallic metasurfaces (MMs) to enhance the gain and directivity of shortened horn antennas. The MM was designed based on the strategy of correcting the actual phase errors probed on the aperture of the horn using the near-field phase-transformation principle. The fundamental unit cell of the MM is made of a pair of cross slots created in a monolithic thin conductive sheet and is entirely free from high-cost dielectrics. The lack of dielectrics makes MM lightweight, cost-efficient and easy to fabricate the prototype for mass production. The MM has a 2D array of unit cells arranged to increase the gain of the shortened horn by improving aperture efficiency through local phase transformation in a wide frequency band. The concept is demonstrated by designing MMs for shortened horns with different heights and the same physical aperture at the center operating frequency of 12.5 GHz. The maximum gain-bandwidth with MM is achieved for the shortest horn, which is validated by measuring the physical prototype. The results indicate that horn gain with MM increases by 9.2 dB (from 11.1 to 20.3 dBi) and has a 3-dB fractional gain-bandwidth of 10.4%. The weighted density of the fabricated MM is only 0.87 g/cm^2. Including MM, the total antenna height is around 61% shorter than a conventional air-filled horn having a similar peak gain.

INDEX TERMS Conical horn, dielectric-free, high-gain, higher directivity, lens, metallic cover, metasurface, metal manufacturing, phase transformation, phase correction, polarization-insensitive, substrate-less, shortened horn.

I. INTRODUCTION

Since late 1800s, the horn antenna has been a microwave choice as a front-end antenna or feed of high-gain antennas such as lenses and dishes for low-cost wireless applications [1]–[7]. To achieve high gain with reduced aperture, horns are made taller, adding extra weight and height to the system. The antenna weight and profile are critical for space-limited modern systems such as CubeSats [8]. The shortened horns with large aperture have limited gain due to dominating quadratic phase distribution errors at the aperture [1]. The gain can be enhanced by improving phase uniformity through an additional phase compensator (PC) [9]. Based on the material used in the implementation, the PC designs reported in the literature can be categorized into all-dielectric, composite, or fully metallic.

Conventional PCs are made of dielectrics, which are thick, bulky and heavy [10], [11]. Thick metamaterial PCs [12], [13] using multilayer dielectric slabs were realized based on effective medium theory. Later, single-layer dielectric PCs were reported with and without additional antireflection layers [14], [15]. Even more complex planar [16] and non-planar

The associate editor coordinating the review of this manuscript and approving it for publication was Derek Abbott.

[17] 3D printed dielectric PCs were also investigated, but such structures are delicate due to the cuboid 3D lattices with thin dielectric interconnectors. The PCs in the second group are typically made of different shapes of conductive patterns printed on multilayer dielectric substrates, which are often bonded together with prepregs [18]–[25]. Despite having exceptional performance, all-dielectric and composite PCs are either tall and heavy or costly. Some 3D printed dielectric based PCs were developed for low-cost applications [26]. However, high radio-frequency losses make them less attractive for practical systems [27]. Furthermore, because dielectrics have a low electric field breakdown threshold, their use in high-power applications is limited.

On the other hand, all-metal PCs eliminate dielectrics and can be used with high-power systems. They do not suffer from excessive losses and can be developed at a low cost. Despite having practical interest, a limited number of all-metal PC designs have been reported in the literature. A class of metal lenses reported in [28] has a concave profile and is made of conducting plates. In [29], [30], metamaterial inspired bulky wire-medium PCs were investigated to improve the gain of shortened horns. The metallic blocks loaded with slow-wave techniques [31], [32] can also enhance the gain of shortened horns. However, block placements of such designs are arbitrary and require a sophisticated metal manufacturing process. In [33], a shortened conical horn antenna with a lightweight all-metal PC has been proposed. The PC comprises two layers of resonators connected diagonally through 0.4 mm thin metallic mesh grids. The structure is mechanically fragile, and fabrication needs extended exposures to the laser beam to remove large metal chunks, often deforming the structure. A 3D printed all-metal PC has recently been demonstrated to successfully improve the wideband gain of a horn [34]. However, the volumetric intricate stepped configuration of such PCs is a bottleneck that can only be fabricated using a specialized technology.

This article presents mechanically robust, fabrication-friendly, fully metallic metasurfaces (MMs) synthesized based on the near-field phase transformation principle [35]. Hence, such PCs can be placed closest to the horn aperture ($\leq \lambda/24$), whereas PCs based on lens theory must maintain a certain focal distance from the feed. The proposed MM is novel in many aspects. The structure is made of four identical thin metal sheets with a 2D array of narrow slots. It uses the concept of creating narrow slots in thin monolithic metal sheets, making the structure mechanically rigid without using any external supports or 3D structures [34]. Unlike PC in [33], removing minimal metal from thin metal sheets in the shape of narrow slots is easy to create with any low-cost metal manufacturing procedures. The fundamental cells of the MM can achieve a nearly continuous phase shift from 0 to 360° while maintaining high transmission magnitude (> -1 dB), whereas cells in [33] have limited phase coverage. The MM does not alter the polarization of the electric field propagation through it and hence can be used both for linearly and circularly polarized base antennas. The MM can be made

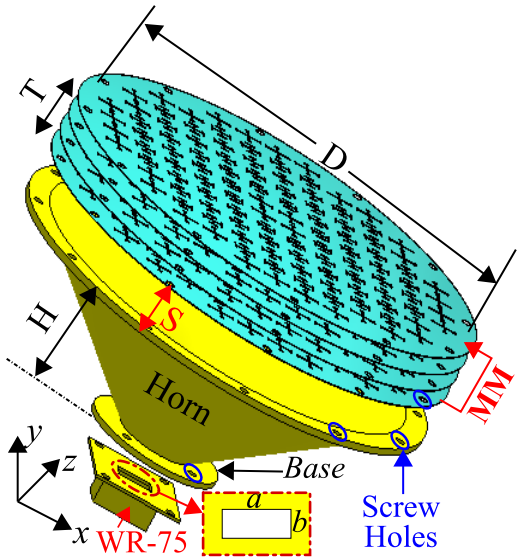

FIGURE 1. A perspective view of the proposed antenna system with an exploded view of a feed adapter. The MM is placed at the horn's aperture at a spacing of S.

out of any planar, inexpensive off-the-shelf thin metal sheets instead of the stepped 3D metallic PCs proposed in [34]. Furthermore, the lack of dielectric reduces the cost and weight significantly and makes the system potential for high-power applications.

The rest of this article is organized as follows. Section II presents the overall configuration of the antenna system and briefly discusses the design principle. The detailed design strategy of shortened horn and MMs are explained in Section III. The improvement in radiation performances of shortened horns with MMs, predicted through full-wave simulations, are compared in Section IV. The prototype and measurement results are discussed in Section V. Finally, Section VI concludes the article.

II. CONFIGURATION OF THE ANTENNA

The configuration of the proposed antenna system is shown in an exploded view in Fig. 1. It has a shortened horn and an MM placed at the aperture of the horn. The aperture size (D) and flare height (H) can be varied with the change in flare angle of the horn. The spacing (S) between horn and MM has a crucial impact on antenna performance and can be defined by the MM's design methodology. The thickness of MM is T, and it is comprised of four identical thin metal sheets where each sheet has arrays of narrow slots. The MM is specially designed to process the electric field locally, leaving the aperture of the horn by improving the phase uniformity. It is worth mentioning that in order to have reflection less field propagation with the shortest S, the MM must be highly transparent.

The horn is excited through a WR-75 waveguide-to-coaxial adapter fixed with an $a \times b$ mm^2 slot (see inset of Fig. 1) at the center of a metal sheet. A 2 mm thick circular

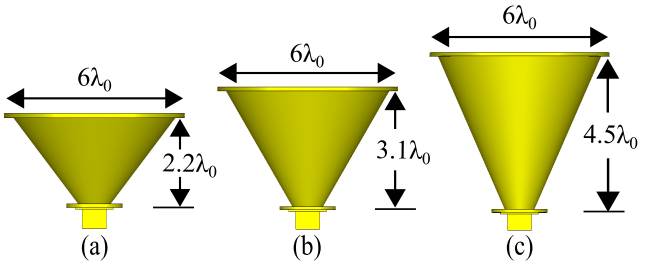

FIGURE 2. Horn configurations with different flare heights and fixed apertures: (a) design I, (b) design II, and (c) design III.

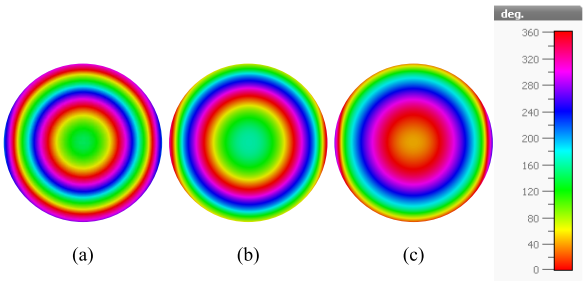

FIGURE 3. Aperture phase distribution (E_y) of shortened horns; (a) design I, (b) design II, and (c) design III.

base with a diameter of 50 mm is attached at the bottom part of the horn to hook up the slotted metal sheet, feed and horn firmly through four pre-cut holes. The top of the horn cone has a 7.6 mm wide extended circular edge with a thickness of 2.4 mm, which is created to securely attach the MM to the horn in the near-field region. For this purpose, the edge-ring has twelve holes separated by an angular spacing of 30°.

III. DESIGN METHODS

The design strategies of customized shortened horns and MM are discussed in this section elaborately.

A. SHORTENED CONICAL HORN

The horn theory has been extensively covered in the literature [1]; only key features necessary to understand the design aspects are discussed here for brevity. The gain, G, of a conical horn can be estimated numerically (1).

$$G = \eta_a \frac{4\pi A_P}{\lambda^2} \tag{1}$$

where η_a is the aperture efficiency, A_p is a physical aperture of the antenna, and λ is the free-space wavelength at the design frequency.

The maximum gain is achieved when the aperture diameter, d_a of horn satisfies $d_a \cong \sqrt{3H\lambda}$ (where H is the axial length of horn) [1]. In principle, the flare angle (or aperture size) and horn height significantly impact the peak gain. Although a larger flare angle provides a higher gain for a given axial length, it limits the gain due to dominating quadratic phase error at the aperture. On the other hand, for a fixed aperture (d_a), its flare length must be sufficiently large to achieve high gain, which is impractical in many volume constraint applications.

To investigate the efficacy of the proposed MM, three customized shortened conical horns have been designed with different heights and fixed apertures, as shown in Fig. 2. The aperture size of the horn is kept fixed at $6\lambda_0$, whereas the flare heights are: $2.2\lambda_0$, $3.13\lambda_0$ and $4.5\lambda_0$, where λ_0 denotes free-space wavelength at the design frequency of 12.5 GHz. Hereafter, the three horns are referred to as Design I, Design II, and Design III.

The three horns were modeled and simulated with the time-domain solver of CST Microwave Studio (MWS). The aperture phase distributions of the dominant electric field (E_y)

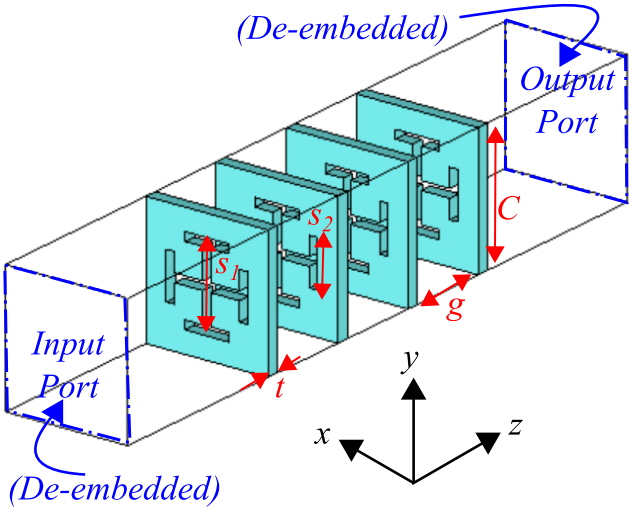

FIGURE 4. The configuration of a fundamental metallic cell used in the MMs.

are shown in Fig. 3 (a-c) for each Design. The maximum phase variations for Design I, II, and III are 415°, 313° and 243°, respectively, which limit their respective peak gains in the broadside direction of 11.1 dBi, 13.2 dBi, and 16.0 dBi. It is worth mentioning that the shortest horn (Design I) has the maximum phase error of 415°, and hence, suffers from the lowest peak gain of only 11.1 dBi. With the expense of horns' height, the gain improves as the phase error reduces.

B. METALLIC METASURFACE (MM)

The phase nonuniformity for the three designs is improved with three different MMs. The MMs are designed using a fundamental metallic cell that can provide a complete 360° phase shift with high transmission magnitude at the operating frequency. A generic configuration of the quad-layer metallic cell used in the MM is shown in Fig. 4. It is built on 0.5 mm narrow slots cut in a thin continuous metal sheet, ensuring mechanical rigidity automatically without using any dielectric substrate or extra 3D and non-electromagnetic (EM) metallic features' support.

Cells of the metallic lattice were analyzed and optimized with periodic boundary conditions and Floquet modes (Fig. 4) in CST MWS. The lateral dimensions of the cells are set to

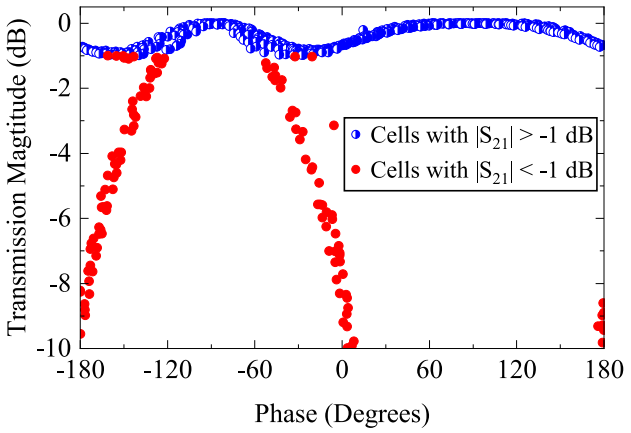

FIGURE 5. The transmission characteristics of the fundamental cells in MM. The length of cross slots S_1 and S_2 in the cells are varied from 6 to 11 mm, and 1 to 5 mm, respectively.

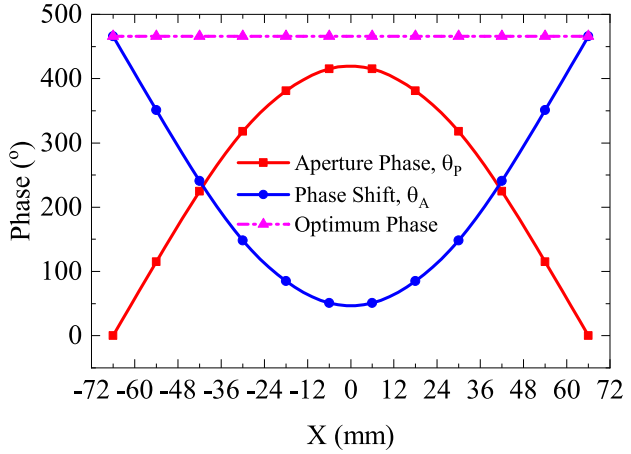

FIGURE 6. Aperture phase distribution and phase shifts are needed through MM for compensating the phase nonuniformity in the aperture.

$C = 12.5$ mm, the air gap between adjacent metal sheets is fixed to $g = 6$ mm, and the metal thickness of each layer is $t = 0.3$ mm. It should be noted that for a complete 360° phase range with a higher transmission magnitude, a quarter-wavelength air gap ($g = \lambda/4$) is considered the optimal distance [36], [37]. The cells' slot lengths (S_1 and S_2) were varied between 6 to 12 mm and 1 to 5 mm, respectively. The transmission magnitude and phase of all the best-selected cells are plotted in Fig. 5. It shows that any phase value between 0 and 360° with reasonable continuity can be achieved while maintaining transmission magnitude > -1 dB (blue dots). This feature is highly desired for phase-shifting cells because phase variation on antenna aperture is often continuous. Moreover, the cell is 90° rotationally symmetric, which makes the MM polarization insensitive.

The next step is to form the MM with metallic cells arranged in a 2D array. In MM design, first, the phase of the field radiated by the horn is probed at its aperture at a spacing of $S = \lambda/24$ using virtual E-probes in full-wave EM

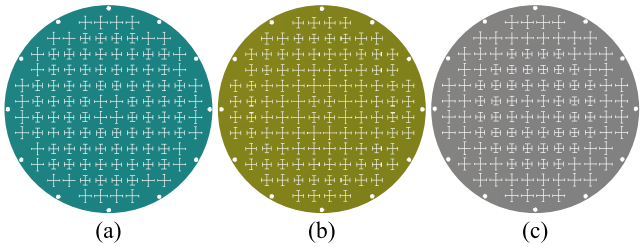

FIGURE 7. The arrangement of cells in the MMs and front layout of MMs for (a) design I, (b) design II, and (c) design III.

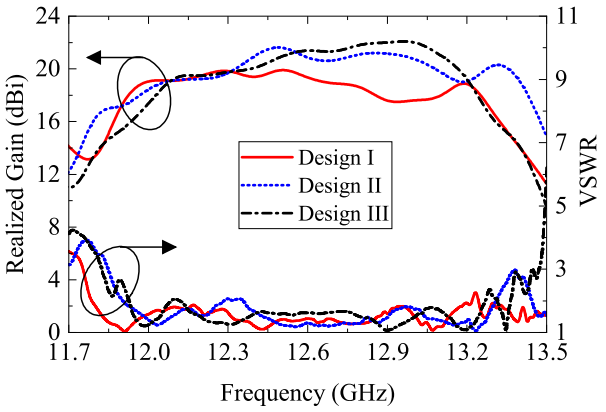

FIGURE 8. The predicted gain and impedance match bandwidths of three shortened horns with their respective MMs.

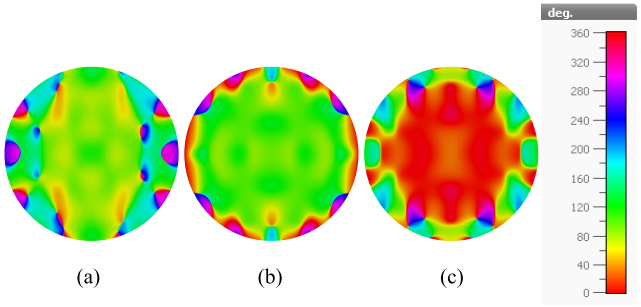

FIGURE 9. Aperture phase distribution (E_y) of shortened horns after using respective MMs with (a) design I, (b) design II, and (c) design III.

simulations. This is done by discretizing the space above the horn aperture into 12×12 cells. The E-field probes are then defined at the centre of each cell to compute the phase of the electric field. A more detailed description of this process is reported in earlier publications [35], [38] and is not repeated here for brevity. It can be seen in Fig. 3 (a-c) that the near-field phase distribution is rotationally symmetric; hence, the phase probed at six (6) discrete radial distance points will be a close approximation and also reduce the design complexity significantly. Therefore, the normalized phases (θ_P) probed along the $+x$-axis at six discrete points for three designs are listed in Table 1. Each best metallic cell is thus selected and incorporated in a specific fashion to form the MM based on the pre-calculated phase shift required at each location. As a

TABLE 1. Slot dimensions and transmission coefficients of metallic cells used to form three different MMs for the respective design I, design II and design III.

	DESIGN I						DESIGN II						DESIGN III					
Cell			Slot dimensions & coefficient						Slot dimensions & coefficient						Slot dimensions & coefficient			
Center	θ_P	θ_I	S_1	S_2	$\lvert S_{21}\rvert$	θ_A	θ_P	θ_I	S_1	S_2	$\lvert S_{21}\rvert$	θ_A	θ_P	θ_I	S_1	S_1	$\lvert S_{21}\rvert$	θ_A
x (mm)	(°)	(°)	(mm)	(mm)	dB	(°)	(°)	(°)	(mm)	(mm)	dB	(°)	(°)	(°)	(mm)	(mm)	dB	(°)
6	415	51	9.6	2.1	-0.11	50	313	37	8.0	3.4	-0.13	39	243	72	8.6	2.8	-0.01	73
18	381	85	7.0	4.1	0.00	83	293	57	10.5	1.4	-0.09	57	227	88	7.8	3.4	0.00	89
30	318	148	7.6	3.4	-0.17	147	247	103	9.0	2.4	-0.01	100	192	123	7.0	4.0	-0.01	124
42	225	241	7.9	2.9	-0.42	240	182	168	8.5	2.6	-0.51	168	142	173	7.4	3.5	-0.57	173
54	115	351	7.8	3.7	-0.78	351	99	251	7.3	3.4	-0.23	252	80	235	9.3	1.8	-0.47	235
66	0	106	9.9	1.7	-0.03	106	0	350	8.7	3.0	-0.83	349	0	315	10.0	2.1	-0.55	316

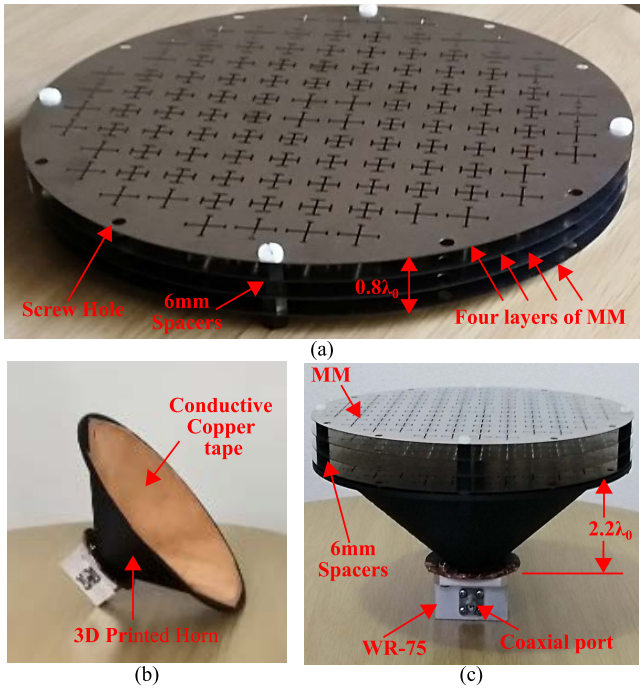

FIGURE 10. Photographs of (a) an assembled MM for the design I, (b) 3D printed copper-tapped shortened horn with coaxial to waveguide adapter feed, and (c) assembled prototype.

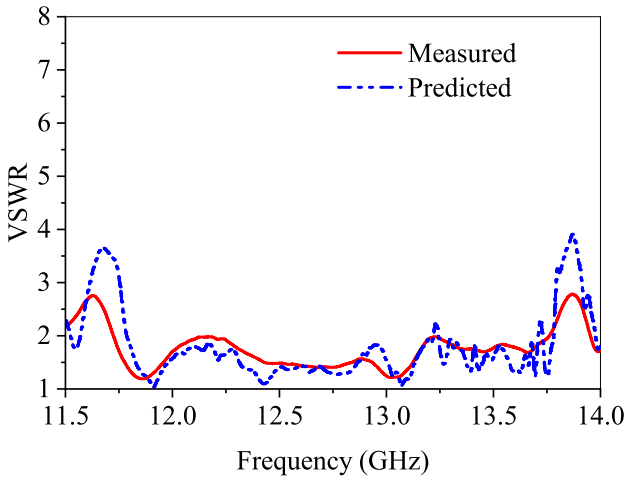

FIGURE 11. Measured and predicted VSWR for the fabricated prototype of shortened horn with MM.

TABLE 2. Performance of design I, II and III with their respective MMs.

Design	Flare Height (λ_0)	Phase Errors (°)	Imp. BW (%)	Peak Gain (dBi) Without MM	Peak Gain (dBi) With MM	3-dB Gain BW (%)	3-dB Beamwidth E-plane	3-dB Beamwidth H-plane
I	2.2	415	11.45	11.1	20.3	10.4	11.2	17.1
II	3.1	315	11.11	13.2	22.0	10.2	12.3	14.4
III	4.5	243	10.64	16.3	22.3	8.7	12.5	16.2

result, each cell in an MM locally manipulates the incoming electric field's phase and shifts it into a desired phase of the outgoing fields resulting in uniform phase distribution at the output plane.

The formation of MM for Design I (shortest horn) is explained in detail here, and others are designed following the same methodology. The non-uniform aperture phase (θ_P) of Design I probed at discrete points is plotted in Fig. 6. The desired uniform phase at the outgoing plane of MM, which can be any constant value, is set to 466°, as shown in Fig. 6. The phase compensation needed at discrete points on the aperture of Design I is simply the difference between desired and existing phase. For example, at position $x = 6$ mm, the aperture non-uniform phase (θ_P) is 415°; hence, $\theta_I = 51°$ ($= 466° - 415°$) phase value is ideally required for the phase compensation.

Against each phase shift value needed for the phase compensation, a cell is selected from the pre-computed cell database (Fig. 5) with the strategy to have the highest transmission magnitude and phase value, θ_A closest to the ideal phase θ_I needed for compensation. For this example, the selected cell has slot dimensions of (S_1, S_2) = (9.6 mm,

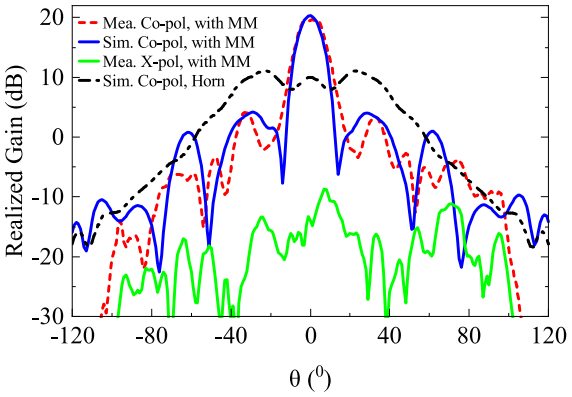

(a) E-plane

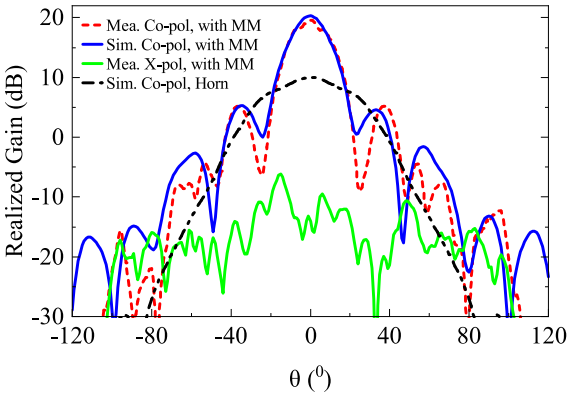

(b) H-plane

FIGURE 12. Measured and predicted far-field pattern cuts of the shortened horn (design I) with and without MM, at 12.5 GHz.

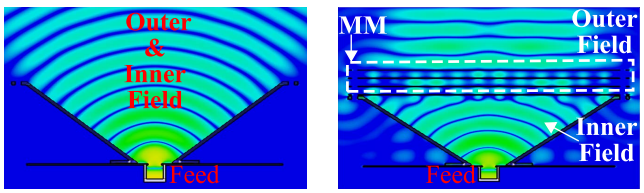

(a) Horn without MM (b) Horn with MM

FIGURE 13. Near-field phase distribution of the dominant field component (E_y) in a cross-section of the shortened horn antenna at 12.5 GHz.

2.1 mm) and has a transmission magnitude and phase of −0.11 dB and 50°, respectively. Subsequently, all other required cells were selected and summarized in Table 1. The cells needed for the phase compensations of Design II and Design III are also listed in Table 1. The least transmission magnitude for the selected cells is −0.83 dB, and the phase deviation is not more than 3°. The top-view of MMs designed from the selected cells is shown in Fig. 7 (a-c). It is to be mentioned here that following rotational symmetry in the aperture phase distribution, selected cells were repeated in the physical MMs equivalent to the aperture of the horn.

IV. PERFORMANCE OF THREE SHORTENED HORNS

Three customized horns with MMs demonstrated in Section III were simulated in CST MWS. The key performances of the three designs are compared and presented in Table 2. With MM, a noteworthy gain improvement of 9.2 dB, 8.8 dB, and 6.0 dB for Design I, II and III, respectively, was achieved. Such gain enhancement of three different shortened horns confirms that the proposed MMs can effectively compensate for the significant phase variations of any shortened horns, thanks to their vital phase compensating ability.

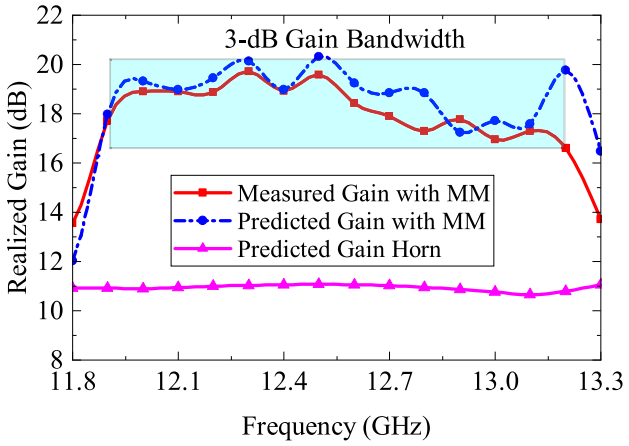

FIGURE 14. The measured and predicted realized gain of the shortened horn (design I) with and without MM over a wide frequency range.

The wideband performances (gain and impedance matching at the antenna input with MMs) are plotted in Fig. 8. Each Design also shows a reasonable wideband gain and impedance matching bandwidths. At VSWR < 2, the impedance bandwidths of Design I, II, and III are 11.45 % (11.78 - 13.21 GHz), 11.11% (11.9 - 13.3 GHz), and 10.64% (11.9 - 13.26 GHz), respectively. The respective 3-dB gain bandwidths are 10.4% (11.9 - 13.2 GHz), 10.2% (12.1 - 13.4 GHz), and 8.7% (12.1 - 13.2 GHz). Design I provides the largest 3-dB gain bandwidth, but it gradually reduces for Design II and Design III with the increasing in horn heights. The aperture phase distributions of the dominant e-field components (E_y) of all three Designs with MMs are plotted in Fig. 9 (a-c). The nearly uniform phase distribution is noted over the aperture in each case.

Furthermore, according to the gain vs horn's length and aperture diameter plot reported in [1], for a fixed aperture diameter of $6\lambda_0$, approximately 189.6 mm ($\approx 7.9\lambda_0$), 237.6 mm ($\approx 9.9\lambda_0$), and 240.0 mm ($\approx 10\lambda_0$) long air-filled conical horn antennas are needed to achieve the gain values of around 20.3 dB, 22.0 dB and 22.3 dB, respectively. These figures indicate a 72.2% (from 189.6 to 53 mm) reduction in the flare height of Design I. The height reductions for Design II and Design III are 68.7% (from 237.6 to 75 mm) and 55% (from 240 to 108 mm), respectively.

V. PROTOTYPE AND MEASUREMENTS

A prototype of the Design I was made and tested experimentally to validate the predicted results. Photographs of the prototyped horn, MM, and the assembled system are shown in Fig. 10.

TABLE 3. Performance comparison of horns with state-of-the-art phase compensator.

Ref.	Freq. (GHz)	PC Types & weight	PC Thickness (λ)	PC Size (λ)	Realized Gain (dB)	Spacing Horn-PC (λ)	Antenna Height (λ)	PC Polarization	Rigidity & Complexity
This work	12.5	Metal Light	0.80	6.0	20.3 (Sim.) 19.7 (Mea.)	0.04	3.0	LP/CP	Robust Low
[34]	30.0	Metal Bulky	3.46	7.5	24.2 (LP) 23.5 (CP)	3.50	10.3	LP/CP	Robust High
[33]	11.0	Metal Light	0.41	4.7	20.46	–	3.0	LP/CP	Delicate High
[29]	10.0	Metal Bulky	*	*	20.5	*	2.2	LP	Medium High
[30]	6.2	Metal Bulky	0.60	3.3	23.0	*	5.1	LP	Medium High
[15]	34.3	Dielectric Moderate	0.88	14.5	28.4	3.43	18.8	LP	Medium High
[16]	12.0	Dielectric Heavy	0.65	4.0	21.5	0.5	10.1	LP	Delicate Moderate
[25]	9.4	Composite Heavy	0.94	6.1	∼25.4	–	9.3	LP	Robust Moderate
[24]	12.5	Composite Moderate	0.08	7.2	22.0	–	3.0	LP	Robust Moderate

'–' data not available, PC—Phase compensator, *embedded multilayer copper wires arrayed across the horn inner space.

A. FABRICATION AND ASSEMBLING

A laser-cut manufacturing procedure was used to fabricate each layer of MM by etching narrow slots in 0.3 mm thick conductive sheets. Twelve additional holes with an angular spacing of 30° were created at the edge in extended metal to assemble the systems. The four layers of MM have suspended above 6 mm plastic spacers with screws to create the precise air gap between adjacent layers, as shown in Fig. 10 (a). The MM has an overall thickness of $0.8\lambda_0$ and a total weight of around 142.4 g only.

For fast prototyping, the conical horn used to demonstrate the operation of the MM was fabricated with a 3D printed technology using acrylonitrile butadiene styrene material. The 3D printed plastic horn's inner surface was then metalized using thin copper tape, as shown in Fig. 10 (b). The overall weight of this 3D printed horn is only 55.5 g. Finally, the assembled MM was stacked on the horn with 1 mm spacers in the system to complete the prototype, as shown in Fig. 10 (c). Including MM, the maximum antenna height is 73.2 mm ($\approx 3.05\lambda_0$).

B. MEASURED RESULTS

The impedance matching at the input of the antenna system was measured using a multi-port vector network analyzer (Agilent PNA-X N5242A). The measured and predicted voltage standing wave ratio (VSWR) is plotted in Fig. 11. The measured impedance bandwidth is around 16% (11.72 - 13.76 GHz) and agrees well with the predicted result obtained through full-wave simulation.

The far-field measurements were carried out in an NSI spherical near-field range. At the design frequency of 12.5 GHz, the measured and predicted pattern cuts of shortened horns with and without MM at two principal planes are compared in Fig. 12. Excellent agreements are noted between measured and predicted pattern cuts with minor discrepancies due to measurement tolerances. The measured peak gain is around 19.6 dBi, and the main beam is directed in the boresight direction. The measured cross-polar component is at least 28 dB below the co-polar component. The sidelobes are 15.6 dB and 14.6 dB below the main beam in the E- and H-plane, respectively. There are 59.3% (27° to 11°) and 63% (46° to 17°) reductions in 3-dB angular beamwidths at E- and H-plane, respectively

The increase in gain for Design I with MM is 8.5 dB due to its increasing uniform phase aperture area. The aperture phase compensations are verified through simulations, as shown in Fig. 13. With MM, the phase fronts are almost parallel (i.e. planar) throughout the aperture (Fig. 13 (b)), whereas it was curved (i.e. spherical) without MM (Fig. 13 (a)).

The broadband performance of Design I was also tested over a frequency range from 11.8 to 13.3 GHz. The measured and predicted gains are plotted in Fig. 14, and a good agreement is noted with a minor discrepancy because of fabrication, assembling and measurement tolerances. The measured 3-dB fractional gain bandwidth is around 10.4% at the center frequency of the operating band, and the maximum peak gain of 19.7 dBi is recorded at 12.3 GHz. At this frequency, the aperture efficiency is 27.2%, which is seven times

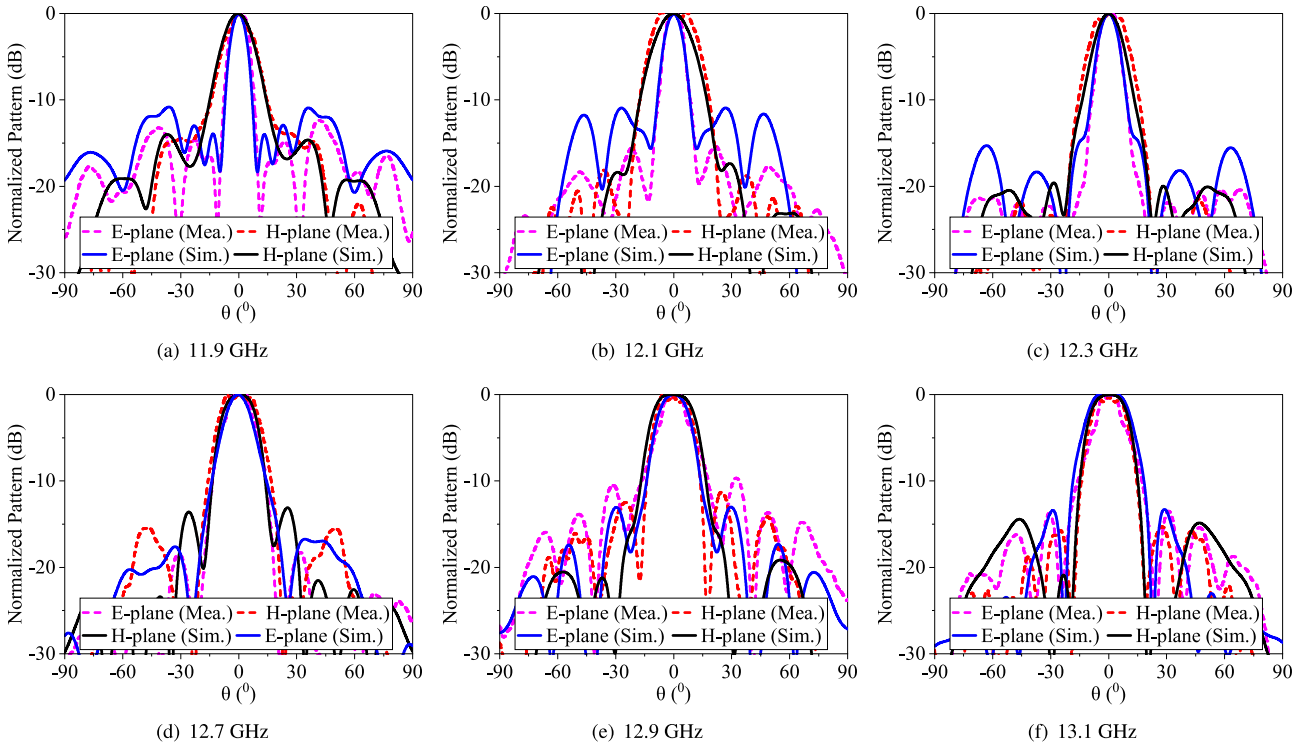

FIGURE 15. The measured and predicted far-field pattern cuts of the antenna system (design I) at two principal planes within the band of interest.

greater than the 3.7% aperture efficiency of the horn without a metasurface. The predicted gain curve of shortened horn without MM is also included in Fig. 14 to show the notable contribution of the proposed MM. Around 5.8 - 8.7 dB gain enhancements are noted throughout the operating band of interest. However, the 3-dB gain bandwidth of the horn with metasurface is reduced compared to that of the horn without metasurface.

The normalized far-field pattern cuts in E- and H-planes at six different frequencies within the band are plotted in Fig. 15. There are good agreements between measured and predicted pattern cuts, and the measured sidelobe levels are acceptably low over the entire band of interest. Overall, the measured results validate the proof of concept of fully metallic metasurfaces to compensate for the phase errors of shortened horn's aperture. Table 3 compares the key performance of the proposed shortened horn to the state-of-the-art designs to assess the MM's efficacy. Table 3 shows that the shortened horn with mechanically robust MM has comparable height and electrical performance. Moreover, such planar polarization invariant MM can be realized through industry-friendly fabrication processes with extremely low-cost, off-the-shelf thin metal sheets.

VI. CONCLUSION

Lightweight, low-cost, mechanically robust MMs are developed, and their potential to compensate for the aperture phase nonuniformity of shortened horn antennas is demonstrated successfully. The design aspect of MM is guided by the physics of near-field phase transformation and built on a knowledge of actual phase errors. Hence the proposed MMs are also equally useful to synthesize and analyze near-field for other applications. The design approach populates a polarization-insensitive MM, and it does not depend on polarization conversion at all. The lack of bulky dielectrics also makes the MM ideal for many industrial applications considering cost, weight, and environmental hazard resistance. The measured results validate the concept and indicate excellent antenna performance. Including MM, a 61% shorter horn antenna was realized, and around 5.8-8.7 dB gain enhancements were achieved with lower sidelobes over a reasonable wide band. The aperture efficiency was improved by 7.35-folds with the excellent cross-polar component rejection capability. Overall, the innovative design approach, system's weight, size, and excellent radiation performance make it attractive and open the door for many possibilities for terrestrial and space applications.

REFERENCES

[1] C. A. Balanis, *Antenna Theory: Analysis and Design*, 3rd ed. Hoboken, NJ, USA: Wiley, 2009.

[2] J. N. Hines, T. Li, and R. H. Turrin, "The electrical characteristics of the conical horn-reflector antenna," *Bell Syst. Tech. J.*, vol. 42, no. 4, pp. 1187–1211, Jul. 1963.

[3] W. J. Wilson, S. H. Yueh, S. J. Dinardo, S. L. Chazanoff, A. Kitiyakara, F. K. Li, and Y. Rahmat-Samii, "Passive active L- and S-band (PALS) microwave sensor for ocean salinity and soil moisture measurements," *IEEE Trans. Geosci. Remote Sens.*, vol. 39, no. 5, pp. 1039–1048, May 2001.

[4] F. R. Varela, J. L. B. S. Martin, and B. G. Iraguen, "Circularly polarized C-band lens-horn antenna for radar remote sensing calibration," in *Proc. 2nd URSI Atlantic Radio Sci. Meeting (AT-RASC)*, May 2018, pp. 1–4.

[5] M. E. Carkaci and M. Secmen, "The prototype of a wideband Ku-band conical corrugated horn antenna with 3-D printing technology," *Adv. Electromagn.*, vol. 8, no. 2, pp. 39–47, Mar. 2019.

[6] J. Ju, W. Zhang, Y. Zhou, and J. Zhang, "A large-size horn antenna for X-band high power microwave radiations," *Rev. Sci. Instrum.*, vol. 90, no. 2, Feb. 2019, Art. no. 026101.
[7] E. Baldazzi, A. Al-Rawi, R. Cicchetti, A. B. Smolders, O. Testa, C. D. J. V. C. Moreno, and D. Caratelli, "A high-gain dielectric resonator antenna with plastic-based conical horn for millimeter-wave applications," *IEEE Antennas Wireless Propag. Lett.*, vol. 19, no. 6, pp. 949–953, Jun. 2020.
[8] J. M. Kovitz, V. Manohar, and Y. Rahmat-Samii, "A spline-profiled conical horn antenna assembly optimized for deployable Ka-band offset reflector antennas in CubeSats," in *Proc. IEEE Int. Symp. Antennas Propag. (APSURSI)*, Jun. 2016, pp. 1535–1536.
[9] R. E. Collin and F. J. Zucker, *Antenna Theory*. New York, NY, USA: McGraw-Hill, 1969.
[10] E. L. Holzman, "A highly compact 60-GHz lens-corrected conical horn antenna," *IEEE Antennas Wireless Propag. Lett.*, vol. 3, pp. 280–282, 2004.
[11] R. J. Bauerle, R. Schrimpf, E. Gyorko, and J. Henderson, "The use of a dielectric lens to improve the efficiency of a dual-polarized quad-ridge horn from 5 to 15 GHz," *IEEE Trans. Antennas Propag.*, vol. 57, no. 6, pp. 1822–1825, Jun. 2009.
[12] F.-Y. Meng, R.-Z. Liu, K. Zhang, D. Erni, Q. Wu, L. Sun, and J. L.-W. Li, "Automatic design of broadband gradient index metamaterial lens for gain enhancement of circularly polarized antennas," *Prog. Electromagn. Res.*, vol. 141, pp. 17–32, 2013.
[13] Z. Tao, W. X. Jiang, H. F. Ma, and T. J. Cui, "High-gain and high-efficiency GRIN metamaterial lens antenna with uniform amplitude and phase distributions on aperture," *IEEE Trans. Antennas Propag.*, vol. 66, no. 1, pp. 16–22, Jan. 2018.
[14] M. K. T. Al-Nuaimi, W. Hong, and Y. Zhang, "Design of high-directivity compact-size conical horn lens antenna," *IEEE Antennas Wireless Propag. Lett.*, vol. 13, pp. 467–470, 2014.
[15] Y. He and G. V. Eleftheriades, "Matched, low-loss, and wideband graded-index flat lenses for millimeter-wave applications," *IEEE Trans. Antennas Propag.*, vol. 66, no. 3, pp. 1114–1123, Mar. 2018.
[16] S. Shrestha, A. A. Baba, S. M. Abbas, M. Asadnia, and R. M. Hashmi, "A horn antenna covered with a 3D-printed metasurface for gain enhancement," *Electronics*, vol. 10, no. 2, pp. 1–12, 2021.
[17] K. V. Hoel, M. Ignatenko, S. Kristoffersen, E. Lier, and D. S. Filipovic, "3-D printed monolithic GRIN dielectric-loaded double-ridged horn antennas," *IEEE Trans. Antennas Propag.*, vol. 68, no. 1, pp. 533–539, Jan. 2020.
[18] Q. Wu, P. Pan, F.-Y. Meng, L.-W. Li, and J. Wu, "A novel flat lens horn antenna designed based on zero refraction principle of metamaterials," *Appl. Phys. A, Solids Surf.*, vol. 87, no. 2, pp. 151–156, Mar. 2007.
[19] X. Chen, H. F. Ma, X. Y. Zou, W. X. Jiang, and T. J. Cui, "Three-dimensional broadband and high-directivity lens antenna made of metamaterials," *J. Appl. Phys.*, vol. 110, no. 4, Aug. 2011, Art. no. 044904.
[20] L. H. Yuan, W. X. Tang, H. Li, Q. Cheng, and T. J. Cui, "Three-dimensional anisotropic zero-index lenses," *IEEE Trans. Antennas Propag.*, vol. 62, no. 8, pp. 4135–4142, Aug. 2014.
[21] Y. He, N. Ding, L. Zhang, W. Zhang, and B. Du, "Short-length and high-aperture-efficiency horn antenna using low-loss bulk anisotropic metamaterial," *IEEE Antennas Wireless Propag. Lett.*, vol. 14, pp. 1642–1645, 2015.
[22] X. Chen and Y. Ge, "Enhancing the radiation performance of a pyramidal horn antenna by loading a subwavelength metasurface," *IEEE Access*, vol. 5, pp. 20164–20170, 2017.
[23] Q. W. Lin and H. Wong, "A low-profile and wideband lens antenna based on high-refractive-index metasurface," *IEEE Trans. Antennas Propag.*, vol. 66, no. 11, pp. 5764–5772, Nov. 2018.
[24] K. Liu, Y. Ge, and C. Lin, "A compact wideband high-gain metasurface-lens-corrected conical horn antenna," *IEEE Antennas Wireless Propag. Lett.*, vol. 18, no. 3, pp. 457–461, Mar. 2019.
[25] H. W. Tian, W. Jiang, X. Li, Z. P. Chen, and T. J. Cui, "An ultrawideband and high-gain antenna based on 3-D impedance-matching metamaterial lens," *IEEE Trans. Antennas Propag.*, vol. 69, no. 6, pp. 3084–3093, Jun. 2021.
[26] T. Hayat, M. U. Afzal, F. Ahmed, S. Zhang, K. P. Esselle, and J. Vardaxoglou, "The use of a pair of 3D-printed near field superstructures to steer an antenna beam in elevation and azimuth," *IEEE Access*, vol. 9, pp. 153995–154010, 2021.
[27] C. Molero, E. Menargues, T. Debogovic, and M. Garcia-Vigueras, "Circuit modelling of metallic dual-band dual-polarized FSS," in *Proc. 49th Eur. Microw. Conf. (EuMC)*, Oct. 2019, pp. 770–773.
[28] W. E. Kock, "Metal-lens antennas," *Proc. IRE*, vol. 34, no. 11, pp. 828–836, Nov. 1946.
[29] S. Hrabar, D. Bonefacic, and D. Muha, "Numerical and experimental investigation of basic properties of wire medium-based shortened horn antennas," *Microw. Opt. Technol. Lett.*, vol. 51, no. 11, pp. 2748–2753, Nov. 2009.
[30] D. Ramaccia, F. Scattone, F. Bilotti, and A. Toscano, "Broadband compact horn antennas by using EPS-ENZ metamaterial lens," *IEEE Trans. Antennas Propag.*, vol. 61, no. 6, pp. 2929–2937, Jun. 2013.
[31] D. Sun and J. Xu, "Compact phase corrected *H*-plane horn antenna using slow-wave structures," *IEEE Antennas Wireless Propag. Lett.*, vol. 16, pp. 1032–1035, 2017.
[32] J.-Y. Deng, R.-Q. Luo, W. Lin, Y. Zhang, D. Sun, X.-M. Zhang, and L.-X. Guo, "Horn antenna with miniaturized size and increased gain by loading slow wave periodic metal blocks," *IEEE Trans. Antennas Propag.*, vol. 69, no. 4, pp. 2365–2369, Apr. 2021.
[33] A. Lalbakhsh, M. U. Afzal, T. Hayat, K. P. Esselle, and K. Mandal, "All-metal wideband metasurface for near-field transformation of medium-to-high gain electromagnetic sources," *Sci. Rep.*, vol. 11, no. 1, pp. 1–9, Dec. 2021.
[34] Y. Cheng, X. Wang, and Y. Dong, "Broadband dual-polarized metal lens with theoretically arbitrarily variable focal diameter ratio using 3D printing technology," *IEEE Trans. Antennas Propag.*, early access, Apr. 7, 2022, doi: 10.1109/TAP.2022.3164217.
[35] M. U. Afzal and K. P. Esselle, "A low-profile printed planar phase correcting surface to improve directive radiation characteristics of electromagnetic band gap resonator antennas," *IEEE Trans. Antennas Propag.*, vol. 64, no. 1, pp. 276–280, Jan. 2016.
[36] A. H. Abdelrahman, A. Z. Elsherbeni, and F. Yang, "Transmission phase limit of multilayer frequency-selective surfaces for transmitarray designs," *IEEE Trans. Antennas Propag.*, vol. 62, no. 2, pp. 690–697, Feb. 2014.
[37] F. Ahmed, M. U. Afzal, T. Hayat, K. P. Esselle, and D. N. Thalakotuna, "A near-field meta-steering antenna system with fully metallic metasurfaces," *IEEE Trans. Antennas Propag.*, early access, Jun. 29, 2022, doi: 10.1109/TAP.2022.3185502.
[38] F. Ahmed, M. U. Afzal, T. Hayat, K. P. Esselle, and D. N. Thalakotuna, "A dielectric free near field phase transforming structure for wideband gain enhancement of antennas," *Sci. Rep.*, vol. 11, no. 1, pp. 1–13, Dec. 2021.

FOEZ AHMED (Graduate Student Member, IEEE) received the B.Sc. (Hons.) and M.Sc. degrees in information and communication engineering from the University of Rajshahi (RU), Rajshahi, Bangladesh, in 2007 and 2009, respectively, and the M.Eng. degree in electrical and computer engineering from the South China University of Technology (SCUT), Guangzhou, China, in 2013. He is currently pursuing the Ph.D. degree with the School of Electrical and Data Engineering, University of Technology Sydney (UTS), Sydney, NSW, Australia.

From 2012 to 2014, he was a Lecturer with the Department of Information and Communication Engineering, RU, where he has been an Assistant Professor, since 2014 (now on study leave). He was also a Lecturer with the Northern University of Bangladesh, Dhaka, Bangladesh, from 2008 to 2009; and King Khalid University, Abha, Saudi Arabia, from 2009 to 2011. His current research interests include high-gain antennas, SATCOM antennas, metasurfaces, frequency-selective surfaces, and far-field pattern synthesis using near-field phase transformation.

Mr. Ahmed was a recipient of several prestigious awards and scholarships, including the Commonwealth-Funded International Research Training Program (iRTP) Scholarship, the International Research Scholarship (IRS) and the Faculty of Engineering and Information Technology (FEIT) Scholarship from the UTS, the Gold Medal from the RU, the Chinese Government Scholarship, the Academic Achievement Award, and the Excellency Award from SCUT.

MUHAMMAD U. AFZAL (Senior Member, IEEE) received the bachelor's degree (Hons.) in electronics engineering and the master's degree in computational science and engineering from the National University of Sciences and Technology (NUST), Islamabad, in 2009 and 2011, respectively, and the Ph.D. degree in electronics engineering from Macquarie University, Australia, in 2017.

He started his professional career as a Laboratory Engineer, in 2010, with the Research Institute for Microwave and Millimetre-Wave Studies (RIMMS), NUST, where he was promoted as a Lecturer, in 2012, which he continued until February 2013. After his Ph.D. degree, he was offered a postdoctorate for three years on a project funded by the Australian Research Council (ARC) through the Discovery Grant Scheme at Macquarie University. He is currently a Research Fellow working with the University of Technology Sydney. He developed the concept of near-field phase transformation during his doctorate research, which was demonstrated to enhance the directivity of low-gain aperture antennas in IEEE TRANSACTIONS ON ANTENNAS AND PROPAGATION paper entitled ''Dielectric phase-correcting structures for electromagnetic band-gap resonator antennas.'' He is the co-inventor of efficient antenna beam-steering technology referred to as near-field meta-steering. This technology received the ''Highly Commended'' Certificate in the five future-shaping research priorities category in the 2017 Academic Staff Awards at Macquarie University. To commercialize the outcomes of his research, he led a team of colleagues in a CSIRO sponsored ON Prime 2, in 2017, a pre-accelerator program designed to commercialize outcomes of academic research in Australia. Apart from the project-specific research, he co-supervised one Ph.D., three master's of research, and several undergraduate thesis students at Macquarie University. He is also working on the development of satellite-terminal antenna technology. His research interests include electromagnetic phase-shifting structures, frequency selective surfaces, and similar metamaterials for microwave and millimeter-wave antenna applications.

Dr. Afzal has received several awards and scholarships, including a merit-based scholarship in six out of eight semesters during the undergraduate degree, a scholarship of complete fee waiver during the postgraduate degree, and the International Macquarie Research Excellence (iMQRES) scholarship towards doctorate study from Macquarie University. He received the Competitive Travel Grant, in 2015, to present his research work at a flagship conference under the Antennas and Propagation Society (APS) in Vancouver, Canada. He assisted in preparing several grant applications, including a successful ARC Discovery Grant, in 2018. He was third CI in a team of five who received a grant of more than $20K from the German Academic Exchange Service in a funding scheme ''Australia–Germany Joint Research Co-Operation Scheme.''

TOUSEEF HAYAT (Graduate Student Member, IEEE) received the B.S. degree in telecommunication engineering from the University of Engineering and Technology Taxila, Taxila, Pakistan, the M.S. degree (Hons.) from the National University of Sciences and Technology (NUST), Islamabad, Pakistan, and the Master of Research (MRes) degree (Hons.) in electronics engineering from Macquarie University, Australia, in 2018, where he is currently pursuing the Ph.D. degree.

His research interests include electromagnetic-bandgap resonant antennas, additive manufacturing of microwave components, phase and amplitude transforming metasurfaces, and dielectric characterization. He received several prestigious awards, including the International Research Training Program Scholarship (iRTP) for the MRes and the International Macquarie University Research Excellence Scholarship (iMQRES) for his Ph.D. degree.

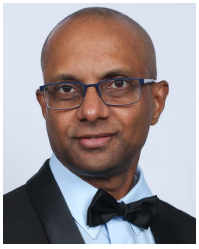

KARU P. ESSELLE (Fellow, IEEE) received the B.Sc. degree (Hons.) in electronic and telecommunication engineering from the University of Moratuwa, Sri Lanka, and the M.A.Sc. and Ph.D. degrees (Hons.) in electrical engineering from the University of Ottawa, Canada.

He is currently a Distinguished Professor of electromagnetic and antenna engineering with the University of Technology Sydney; and a Visiting Professor with Macquarie University, Sydney. According to 2019 special report on research published by The Australian national newspaper, he is the national research field leader in Australia in both microelectronics and electromagnetisms fields. Previously, he was the Director of the WiMed Research Centre; and an Associate Dean of Higher Degree Research (HDR) of the Division of Information and Communication Sciences and directed the Centre for Collaboration in Electromagnetic and Antenna Engineering, Macquarie University. He has also served as a member for the Dean's Advisory Council and the Division Executive and as the Head of the department several times. He has authored approximately 600 research publications and his papers have been cited over 10,000 times. In 2019, his publications received 1,200 citations. He is the first Australian antenna researcher ever to reach Google Scholar H-index of 30 and his citation indices have been among the top Australian antenna researchers for a long time (at present: i10 is 182 and H-index is 49). He is in world's top 100,000 most-cited scientists list by Mendeley Data. Since 2002, his research team has been involved with research grants, contracts, and Ph.D. scholarships worth about 20 million dollars, including 15 Australian Research Council Grants, without counting the 245 million-dollar SmartSat Corporative Research Centre, which started in 2019. His research has been supported by many national and international organizations, including the Australian Research Council, Intel, the U.S. Air Force, Cisco Systems, Hewlett-Packard, the Australian Department of Defence, the Australian Department of Industry, and German and Indian governments.

Dr. Karu is a fellow of the Royal Society of New South Wales (NSW) and Engineers Australia. He was one of the two finalists for 2020 Australian Eureka Prize for Outstanding Mentor of Young Researchers. He received the 2019 Motohisa Kanda Award from IEEE, USA, for the most cited paper in IEEE TRANSACTIONS on ELECTROMAGNETIC COMPATIBILITY in the past five years; the 2019 Macquarie University Research Excellence Award for Innovative Technologies; the 2019 ARC Discovery International Award; the 2017 Excellence in Research Award from the Faculty of Science and Engineering; the 2017 Engineering Excellence Award for Best Innovation; the 2017 Highly Commended Research Excellence Award from Macquarie University, the 2017 Certificate of Recognition from IEEE Region 10; the 2016 and 2012 Engineering Excellence Awards for Best Published Paper from IESL NSW Chapter; the 2011 Outstanding Branch Counsellor Award from IEEE; the 2009 Vice Chancellor's Award for Excellence in Higher Degree Research Supervision; and the 2004 Innovation Award for Best Invention Disclosure. His mentees have been awarded many fellowships, awards, and prizes for their research achievements. 53 international experts who examined the theses of his Ph.D. graduates ranked them in the top 5% or 10%. Two of his recent students were awarded Ph.D. degree (Hons.) at Macquarie University—the Vice Chancellor's Commendation. He has provided expert assistance to more than a dozen companies, including Intel; the Hewlett Packard Laboratory, USA; Cisco Systems, USA; Audacy, USA; Cochlear; Optus; ResMed; and Katherine-Werke, Germany. His team designed the high-gain antenna systems for the world's first entirely Ka-band CubeSat made by Audacy and launched to space by SpaceX, in December 2018. This is believed to be the first Australian-designed high-gain antenna system launched to space, since CSIRO-designed antennas in Australia's own FedSat launched in 2002. He is in the College of Expert Reviewers of the European Science Foundation, from 2019 to 2022; and has been invited to serve as an International Expert/Research Grant Assessor by several other research funding bodies as well, including the European Research Council and funding agencies in Norway, Belgium, The Netherlands, Canada, Finland, Hong Kong, Georgia, South Africa, and Chile. He has been invited by the vice-chancellors of Australian and overseas universities to assess applications for promotion to professorial levels. He has also been invited to assess grant applications submitted to Australia's most prestigious schemes such

as Australian Federation Fellowships and Australian Laureate Fellowships. In addition to the large number of invited conference speeches he has given, he has been an Invited Plenary/Extended/Keynote Speaker of several IEEE and other conferences and workshops, including EuCAP 2020, Copenhagen, Denmark; URSI'19, Seville, Spain; and 23rd ICECOM 2019, Dubrovnik, Croatia. Since 2018, he has been chairing the prestigious Distinguished Lecturer Program Committee of the IEEE Antennas and Propagation (AP) Society—the premier global learned society dedicated for antennas and propagation, which has close to 10,000 members worldwide. After two stages in the selection process, he was also selected by this society as one of two candidates in the ballot for 2019 president of the society. Only three people from Asia or Pacific apparently have received this honor in the 68-year history of this society. He is also one of the three distinguished lecturers (DLs) selected by the society, in 2016. He is the only Australian to chair the AP DL Program ever, the only Australian AP DL in almost two decades, and second Australian AP DL ever (after UTS Distinguished Visiting Professor Trevor Bird). He has been continuously serving the IEEE AP Society Administrative Committee in several elected or ex-officio positions, since 2015. He is also the Chair of the Board of management of Australian Antenna Measurement Facility; and was the Elected Chair of both IEEE NSW and IEEE NSW AP/MTT Chapter, in 2016 and 2017. He is the Track Chair of IEEE AP-S 2020, Montreal; the Technical Program Committee Co-Chair of ISAP 2015, APMC 2011, and TENCON 2013; and the Publicity Chair of ICEAA/IEEE APWC 2016, IWAT 2014, and APMC 2000. He is an Associate Editor of IEEE TRANSACTIONS ON ANTENNAS AND PROPAGATION, *IEEE Antennas and Propagation Magazine*, and IEEE ACCESS. His research activities are posted in the web at: http://web.science.mq.edu.au/~esselle/ and https://www.uts.edu.au/staff/karu.esselle.

DUSHMANTHA N. THALAKOTUNA (Senior Member, IEEE) received the B.Sc. degree in electronics and telecommunication from the University of Moratuwa, Sri Lanka, in 2008, and the Ph.D. degree in electronic engineering from Macquarie University, Australia, in 2012.

He is currently a Lecturer with the School of Electrical and Data Engineering, University of Technology Sydney, Australia. From 2013 to 2019, he has worked in multiple radio frequency and systems engineering roles designing antennas and MMICs and RF systems for both commercial and defense industries. His current research interests include MMICs, SATCOM antennas, base station antennas, reconfigurable microwave and millimeter wave circuits, metasurfaces, and periodic structures. He is a member of the Antennas and Propagation Society and Microwave Theory and Techniques Society and also serves as the Secretary for the IEEE NSW Section.